

引用格式:毛沛宁,黄兴民,吕超,等.基于两步临界退火调控热轧含铝中锰钢的显微组织和力学性能[J].材料工程,2026,54(3):170-180.

MAO Peining, HUANG Xingmin, LYU Chao, et al. Microstructure and mechanical property regulation of hot-rolled Al-contained medium-Mn steel by double intercritical annealing[J]. Journal of Materials Engineering, 2026, 54(3): 170-180.

基于两步临界退火调控热轧含铝中锰钢的 显微组织和力学性能

毛沛宁¹,黄兴民^{1*},吕超¹,刘俊杰¹,张娟²

(1 西南交通大学 材料科学与工程学院 材料先进技术教育部重点实验室,成都 610031;

2 西南交通大学 力学与航空航天学院 应用力学与结构安全重点实验室,成都 610031)

摘要:热轧淬火态中锰实验钢的初始显微组织通常由板条马氏体基体和极少量粒状奥氏体构成,存在明显的Mn偏析带。采用两步(750℃×1h+700℃×1h)临界退火工艺,在不显著改变残余奥氏体含量的前提下,通过分阶段控制富锰区和贫锰区的奥氏体逆转变程度,有效地促进残余奥氏体晶粒细化及机械稳定性的梯度分布。结果表明:在单轴拉伸过程中诱导了更充分和持续的应变诱发马氏体相变。通过相变/孪晶诱发塑性效应协同增韧,最终获得优异强度和韧性匹配,断后伸长率和强塑积达到85.3%和73.4 GPa·%。

关键词:两步临界退火;含铝中锰钢;Mn偏析;残余奥氏体;机械稳定性

doi: 10.11868/j.issn.1001-4381.2023.000733 **CSTR:** 32421.14.j.issn.1001-4381.2023.000733

中图分类号: TG142;TB31 **文献标识码:** A **文章编号:** 1001-4381(2026)03-0170-11

Microstructure and mechanical property regulation of hot-rolled Al-contained medium-Mn steel by double intercritical annealing

MAO Peining¹,HUANG Xingmin^{1*},LYU Chao¹,LIU Junjie¹,ZHANG Juan²

(1 Key Laboratory of Advanced Technologies of Materials, Ministry of Education, School of Materials Science and Engineering, Southwest Jiaotong University, Chengdu 610031, China; 2 Applied Mechanics and Structure Safety Key Laboratory of Sichuan Province, School of Mechanics and Aeronautics and Astronautics, Southwest Jiaotong University, Chengdu 610031, China)

Abstract: Usually, the initial microstructure of hot-rolled and quenched medium-manganese experimental steel is composed of lath martensite matrix and a small amount of tiny granular austenite, also existing apparent Mn-segregation bands. Using double intercritical annealing (holding 60 min at 750 °C followed by 60 min at 700 °C), austenite reversion transformation in Mn-rich and Mn-lean regions are modulated by stages, which efficiently promoting the refinement of retained austenite grains and the optimization of mechanical stability distribution without apparent variation of volume fraction of retained austenite. The results show that adequate and sustained strain-induced martensite transformation is favored and boosted during uni-axial tensile deformation. Due to synergistic toughening of transformation and twinning induced plasticity effects, excellent combination of strength and ductility, such as the ultra-high total elongation of 85.3% and product of strength and plasticity (PSE) of 73.4 GPa·% are obtained eventually.

Key words: double intercritical annealing; Al-contained medium-Mn steel; Mn segregation; retained austenite; mechanical stability

随着社会经济发展和科技进步,能耗、环保、安全等问题日趋严峻。作为第三代先进高强钢的中锰钢

(medium manganese steel, MMS),具有高强度、良好的塑性和低成本等优点,在汽车领域展现良好的应用

前景^[1-4]。传统中锰钢^[5-8]具有典型的多相(multi-phase)、亚稳(meta-stable)、多尺度(multi-scale)(简称M³)组织特征,主要包括铁素体和残余奥氏体(20%~40%,体积分数),后者在形变过程中转变为马氏体,从而延缓颈缩,提升钢的延展性,即相变诱发塑性(transformation induced plasticity, TRIP)效应。研究表明,通过适当的临界退火处理^[9],Fe-C-Mn-Al系中锰钢的强塑积(product of strength and elongation, PSE)超过 60 GPa·%。普遍认为,获得优异的强度和塑性匹配的前提是足量而持续的 TRIP 效应和孪晶诱发塑性(twinning induced plasticity, TWIP)效应协同增韧。残余奥氏体含量(volume fraction of retained austenite, V_{RA})、机械稳定性^[10-11]尤为关键,后者取决于元素含量^[12]、晶粒形态^[13]、尺寸^[5]和取向^[14],可以通过成分设计^[14-15]、温轧^[16]或多步退火^[17]等多种手段进行调控。

Han 等^[18]研究指出,Fe-9Mn-0.05C(质量分数/% ,下同)热轧淬火钢经过临界退火(inter-critical annealing, IA)处理后得到临界铁素体和残余奥氏体,后者具有多边形、板条状等晶粒形态和双模尺寸分布。Zhang 等^[19]采用两步临界退火工艺处理 Fe-0.18C-7.8Mn-1.65Al-0.04Ce 冷轧钢,获得了尺寸分布更宽的板条状和粒状混晶组织,抗拉强度、伸长率和强塑积由 872 MPa、31.48% 和 27.45 GPa·% 提升至 923 MPa、45% 和 41.53 GPa·%。Xu 等^[17]采用两步临界退火处理对 Fe-6.4Mn-2.8Al-0.18C 热轧钢的 V_{RA} 和等轴/条状形貌比进行合理调控,将抗拉强度从 752 MPa 提升至 954 MPa。Zou 等^[20]研究了采用两步退火工艺获得的 Fe-0.01C-5.3Mn-1.53Si-0.56Ni-0.12(Nb+V+Ti)实验钢双相组织中奥氏体稳定性与冲击韧性的关系,发现冲击韧性的增强和微裂纹扩展的抑制与两步工艺引入的 V_{RA} 有关。Hu 等^[21]将两步退火工艺引入渗碳体颗粒作为逆相奥氏体核,促进了内部形成 Mn 梯度的奥氏体晶粒,影响了 V_{RA} 和稳定性,优化了力学性能。上述工作均证实了两步分阶段临界退火调控残余奥氏体含量和机械稳定性梯度的有效性。

众所周知,热轧中锰实验钢在两相区(A_{c1}~A_{c3})保温过程中发生了奥氏体逆转变(austenite reversion transformation, ART)^[22-24]和元素配分(C、Mn 由 α 或 α' 向 γ 富集)^[25]。Lee 等^[26]认为对于 Fe-0.1C-10Mn-1Si-0.3Mo-0.5V 实验钢,Mn 元素的富集相比晶粒尺寸而言对奥氏体稳定性影响更大,富 Mn 带内奥氏体能够发生连续的应变诱发相变。陈学双等^[27]对含偏析带的热轧中锰钢进行临界退火处理,通过合理控制非偏析带区的逆奥氏体转变程度,获得了超高强塑积(PSE > 70 GPa·%)。虽然人们已经逐渐认识到 Mn

元素分布的区域差异及其对进一步提升中锰钢性能的意义,但相关工作主要是针对 Mn 含量(7%~11%)相对较高的实验钢。如前所述,采用温轧、临界退火等工艺引入多种晶粒形态和尺寸双模分布,低锰含量(3%~6%)含铝中锰钢也获得了优异的强韧匹配,并因其相对较低的成本而展现出更强的应用前景。现有工作更多关注如何提高奥氏体含量、实现机械稳定性的合理梯度分布^[28],以及通过持续而充分的 TRIP 效应^[29]、异质结构强化^[30]、TWIP 效应^[31]等实现协同强韧,与此同时,轧态实验钢元素分布及其对组织调控的影响鲜有表述,相关文献报道相对较少。低锰含量(3%~6%)含铝中锰钢是否存在类似 Mn 偏析带,与通过临界退火等热处理获得的非均质结构(比如多种晶粒形态^[19]和双模尺寸分布^[17])之间存在何种关联,有待进一步研究。本工作选取 Fe-5Mn-3.2Al-0.35C 热轧淬火钢,从 Mn 偏析和组织演变等角度分析两步临界退火处理对显微组织和力学性能的影响,以期为新型高强韧中锰钢的开发应用提供借鉴和参考。

1 实验材料与方法

1.1 实验材料

按设计名义成分 Fe-5Mn-3.2Al-0.35C 称量配料,采用 ZG-25 型真空中频感应熔炼炉在真空背底和氩气保护下熔炼浇铸获得钢锭,在 1250 °C 均匀化退火 2 h,经自由锻造得到固定截面尺寸(100 mm×30 mm)板坯,空冷至室温;而后将板坯快速升温至 1200 °C 再保温 2 h,在 850~880 °C 之间经 7 道次轧制得到 5 mm 厚钢板,空冷至室温。使用 OBLF750 型火花直读光谱仪测试实验钢的化学成分,如表 1 所示。

表 1 实验钢设计和实测化学成分(质量分数/%)

Table 1 Designed and measured chemical compositions of experimental steels (mass fraction/%)

Composition	Mn	Al	C	Fe
Designed	5.00	3.20	0.35	Bal.
Measured	4.92	3.21	0.36	Bal.

1.2 实验方法

使用 Thermo-Calc 热力学计算软件和 TCFE6 数据库计算得到实验钢热力学平衡相图,见图 1(a)。由图 1(a)可知,A_{c1}和 A_{c3}分别为 672 °C 和 995 °C,渗碳体(cementite, θ)析出和溶解的温度分别为 677 °C 和 707 °C。本工作采用的临界退火温度(750 °C 和 700 °C)对应的平衡态奥氏体含量分别为 50.34% 和 24.72%,700 °C 可能存在少量渗碳体。

使用SG2-5-12型马弗炉对热轧淬火(用HR代表)钢板进行两步临界退火处理。首先,将实验用钢板随炉升温(后同)至750℃保温1h后水淬至室温,获得一次临界退火态实验钢;而后再置于炉中升温至700℃,分别保温10min和60min后水冷至室温,获得

两步临界退火态实验钢。对不同临界退火态实验钢在200℃下保温20min后水淬,以消除应力。为方便后文叙述,将一次和两步临界退火实验钢分别编号为IA750和DIA700-XX,XX对应保温时间。上述热处理工艺路线见图1(b)。

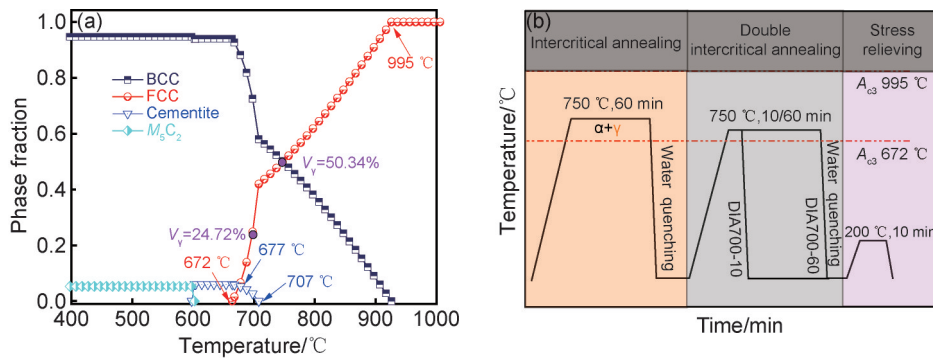


图1 实验钢热力学平衡相图(a)及热处理工艺路线图(b)

Fig.1 Thermodynamic equilibrium diagram(a) and heat-treatment process roadmap(b) of experimental steel

沿着轧制方向电火花线切割取样,依照GB/T 228—2021加工成标准板状拉伸试样,平行段尺寸为40 mm×12.5 mm×4 mm(长×宽×厚)。采用CMT-5305型万能试验机测试样品的室温单轴拉伸性能,应变速率为0.001 s⁻¹。使用D/max-2500/PC型X射线衍射仪获得不同样品截面XRD图谱。扫描范围为40°~110°,扫描速率为2(°)/min。选取(200)_γ、(200)_α、(220)_γ、(220)_α和(311)_γ衍射峰相对积分强度(五峰法)^[32]计算V_{RA}。

使用400至1500目金相砂纸依次将样品打磨至镜面,使用体积分数为4%的硝酸酒精溶液进行蚀刻,在ZEISS SUPRA55型场发射扫描电子显微镜下进行形貌观察,加速电压为20 kV。用0.25 μm粒度Al₂O₃悬浮液将样品抛光至镜面,用酒精迅速擦拭至光亮,采用FEI Quanta 650型场发射扫描电镜进行电子背散射衍射(EBSD)测试,加速电压、工作距离和步长分别为20 kV、20 mm和50 nm,使用JXA-8230型号电子探针显微分析仪(EPMA)获得实验钢样品截面(TD-ND)元素分布情况。TEM测试用样品先机械抛光至50~80 μm厚,在30 V和-30℃下用体积分数为5%的高氯酸和95%的乙醇溶液电解质双喷减薄并冲压成圆片。采用JEOL-2100型透射电镜分析实验钢的微观组织结构,加速电压为200 kV。

2 结果与分析

2.1 微观组织特征

图2为热轧淬火实验钢的组织结构和元素分布。

如图2(a)所示,热轧淬火实验钢主要由板条马氏体构成,板条厚度在0.1~0.3 μm之间。图2(b)EBSD相图证实了极少量(体积分数约2%)粒状残余奥氏体的存在,而图2(c)IPF图呈现出原奥氏体晶界(prior austenite grain boundaries, PAGBs)特征。黑色为未解析和低解析率区域,由热轧淬火过程中马氏体相变产生的内应力所致。图2(d)XRD图谱中仅展现出(110)_α、(200)_α、(211)_α、(220)_α等铁素体或马氏体衍射峰。图2(e)Mn元素分布图表明,热轧淬火态存在带状Mn元素富集(黑色虚线方框),对应区域Al元素含量较低(图2(f))。

图3(a-1), (b-1), (c-1)依次为IA750、DIA700-10和DIA700-60实验钢SEM照片。IA750的显微组织相对均匀,主要为黑色下凹的临界铁素体(α_{1A})和细长板条状奥氏体(γ_L) (图3(a-1)中插图所示)。DIA700-10中可观测到相当数量的块状奥氏体(γ_B)以及沿奥氏体边界析出的细小白色颗粒(图3(b-1)中插图所示)。DIA700-60同样具有块状和板条状两种奥氏体形态,其间仍可见极少量白色颗粒,推断为未完全溶解渗碳体(θ),从文献报道^[33]和热力学计算结果(图1(a))得到印证。两相区保温初期,C、Mn原子受高密度位错钉扎,碳化物析出被抑制^[34];随着时间延长,位错密度下降,C、Mn原子扩散速率增大,马氏体转变为铁素体和渗碳体;而后粒状渗碳体逐渐溶解,因富含合金元素而成为后续奥氏体逆转变的形核点^[35],最终对晶粒形态和尺寸产生重要影响。Image Pro软件统计结果表明,奥氏体板条宽度分别为(0.68±0.08) μm (IA750)、(0.56±0.11) μm (DIA700-10)、(0.56±0.14) μm (DIA700-60)。

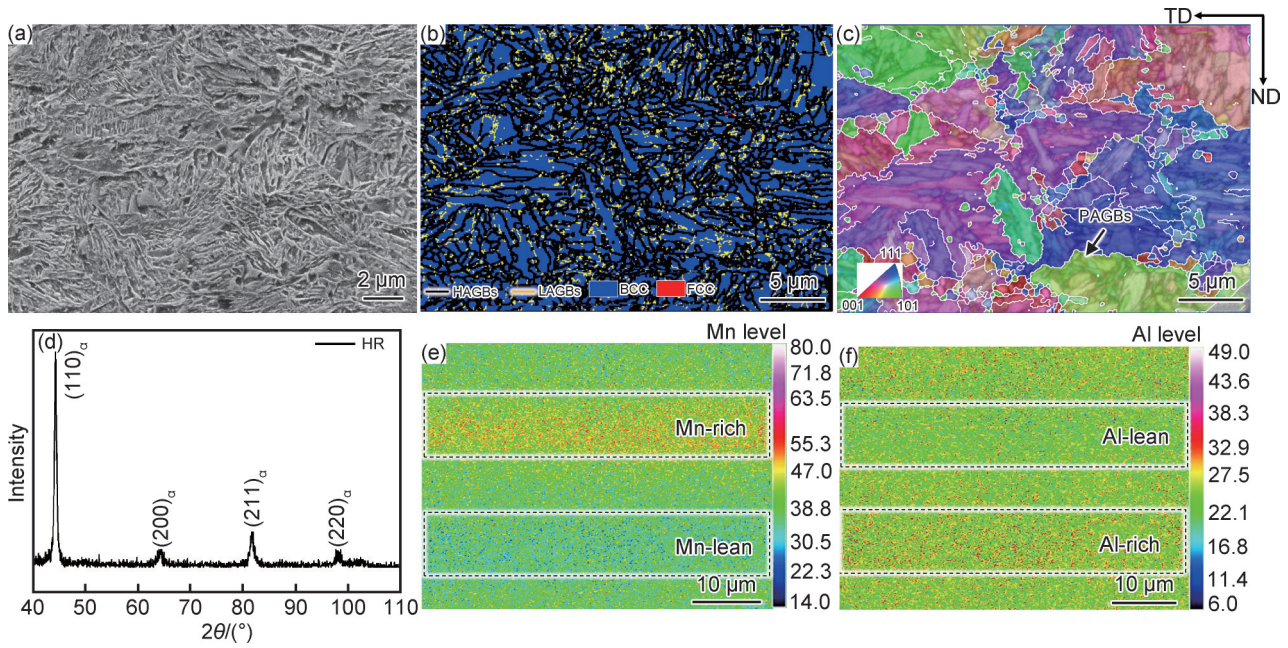


图2 热轧淬火实验钢的组织结构和元素分布

(a)SEM显微照片;(b)EBSD相图;(c)晶粒取向分布图;(d)XRD图谱;(e)Mn元素分布图;(f)Al元素分布图

Fig.2 Microstructure and elements distribution of hot-rolled and quenched experimental steel

(a)SEM micrograph;(b)EBSD phase map;(c)IPF map;(d)XRD pattern;(e)Mn element distribution map;(f)Al element distribution map

图3(a-2), (b-2), (c-2)为三种实验钢截面EBSD相分布图,由体心立方的 α -铁素体或 α' -马氏体(蓝色)和面心立方的 γ -奥氏体(红色)等两相构成,与SEM结果(图3(a-1), (b-1), (c-1))一致。IA750的奥氏体晶粒形态多为板条状,取向杂乱,尺寸不一。DIA700-10和DIA700-60中奥氏体晶粒形态和疏密程度呈现出区域差别,其尺寸与Mn偏析带(图2)宽度相当;DIA700-60的奥氏体密集区内板条晶粒趋于细化,奥氏体稀疏区内晶粒多为粗大条块状。由于晶粒形状不规则,本工作采用面积法统计晶粒尺寸,奥氏体平均晶粒尺寸分别为 $(0.561 \pm 0.053) \mu\text{m}^2$ (IA750)、 $(0.447 \pm 0.105) \mu\text{m}^2$ (IA700-10)、 $(0.381 \pm 0.041) \mu\text{m}^2$ (DIA700-60),铁素体平均晶粒尺寸分别为 $(0.580 \pm 0.053) \mu\text{m}^2$ (IA750)、 $(0.531 \pm 0.122) \mu\text{m}^2$ (IA700-10)和 $(0.622 \pm 0.027) \mu\text{m}^2$ (DIA700-60)。由此可见,相比一次临界退火处理(IA750),两步临界退火(DIA700-60)细化板条奥氏体,促进铁素体/马氏体粗化,导致了不同区域的组织和形态差异(奥氏体富集和稀疏)。图3(a-3), (b-3), (c-3)为不同实验钢的奥氏体晶粒取向,白色虚线勾勒出PAGBs或包界,包内具有相同或相近的晶体学取向,反映出奥氏体逆转变的“记忆效应”^[36]。

图4(a)为三种临界退火实验钢拉伸前后的XRD图谱,可见典型 γ 、 α 或 α' 等多个衍射峰。图4(b)为不同实验钢拉伸试样断口附近的残余奥氏体含量和转

化率统计图,拉伸前 V_{RA} 分别为42.7% (IA750)、41.1% (DIA700-10)和42.4% (DIA700-60),拉伸后 V_{RA} 降至8.6% (IA750)、5.7% (DIA700-10)和2.0% (DIA700-60),对应的形变诱发马氏体相变(strain-induced martensite transformation, SIMT)的转化率分别为79.8% (IA750)、86.1% (DIA700-10)和95.4% (DIA700-60),表明DIA700-60获得更加显著的TRIP效应。

2.2 拉伸力学性能

三种临界退火实验钢的工程应力-应变曲线均为连续屈服,如图5(a)所示。IA750表现出明显的加工硬化和均匀塑性变形;对DIA700-10和DIA700-60而言,当工程应变超过40%时,存在明显锯齿状应力流变^[37]。表2列出了拉伸力学性能参数,IA750的屈服强度(YS)和抗拉强度(UTS)分别为550 MPa和950 MPa,断后总伸长率(total elongation, TE)和强塑积(PSE)分别为71.2%和67.6 GPa·%, DIA700-60的YS和UTS分别为601 MPa和860 MPa, TE与PSE分别达到85.3%和73.4 GPa·%。值得注意的是, DIA700-60的断后伸长率相对IA750得到大幅提升,与更充分的TRIP效应密不可分(图4(b))。图5(b)~(d)为IA750、DIA700-10和DIA700-60临界退火实验钢的真应力-应变和加工硬化率(work hardening rate, WHR)曲线,可分三个阶段。在S1阶段, WHR急剧降低,对应着低位错密度的铁素体快速变形软化^[38];在

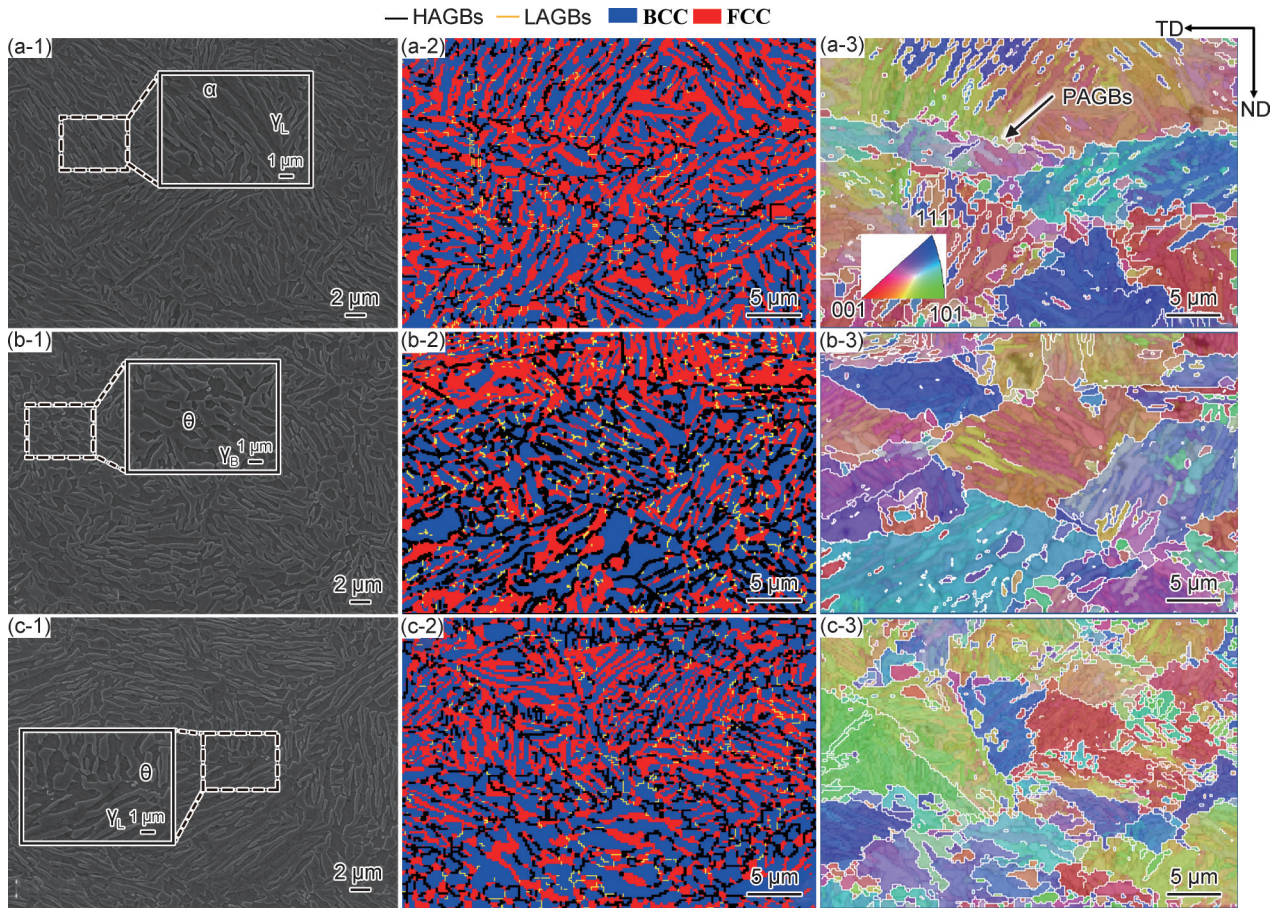


图3 三种临界退火实验钢的SEM照片(1)、EBSD相图(2)和相应的晶粒取向分布图(3)
(a)IA750;(b)DIA700-10;(c)DIA700-60

Fig.3 SEM micrographs(1), EBSD phase maps(2) and corresponding IPF maps(3) of three IA-processed experimental steels
(a)IA750;(b)DIA700-10;(c)DIA700-60

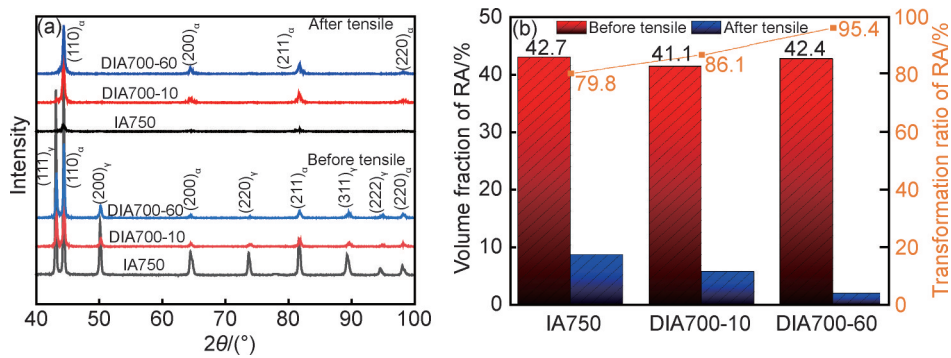


图4 三种临界退火实验钢变形前及拉伸断口处XRD结果
(a)XRD图谱;(b)残余奥氏体含量及转变率

Fig.4 XRD patterns of undeformed sample and tensile fracture of three IA-processed experimental steels
(a)XRD pattern;(b)volume fraction and transformation ratio of RA

S2阶段, WHR缓慢下降,为铁素体变形软化和少量SIMT叠加所导致^[39];在S3阶段,WHR急剧波动,意味着持续而集中的SIMT以及软(α)硬(α')相协同变形^[40]。塑性变形前期(S1和S2),三种临界退火实验钢的真实应变宽度($\Delta\epsilon$)基本相同,分别为0.023和0.267;变形后期(S3)的 $\Delta\epsilon$ 差异较大,分别为0.247(IA750)、0.236

(DIA700-10)和0.312(DIA700-60)。

3 分析讨论

3.1 强韧机制

如前所述,本实验条件下DIA700-60具有最为优

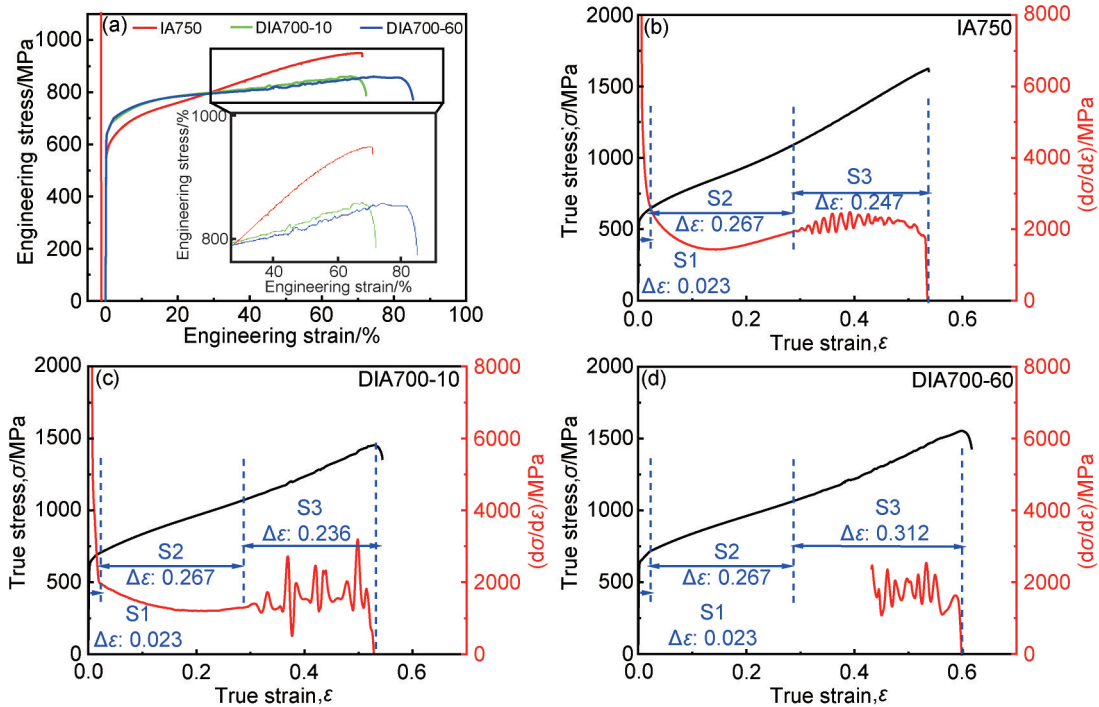


图 5 三种临界退火实验钢的工程应力-应变曲线(a)和加工硬化曲线(b)~(d)

Fig.5 Engineering stress-strain curves(a) and corresponding work-hardening curves(b)-(d) of three IA-processed experimental steels

表 2 三种临界退火实验钢的组织特征和拉伸力学性能参数

Table 2 Microstructure characteristics and tensile mechanical properties parameters of three IA-processed experimental steels

Sample	$V_{RA}/\%$		Transformation ratio/ $\%$	YS/MPa	UTS/MPa	TE/ $\%$	PSE/($GA \cdot \%$)
	Undeformed	Near fracture					
IA750	42.7	8.6	79.8	550	950	71.2	67.6
DIA700-10	41.1	2.8	86.1	580	862	72.5	62.3
DIA700-60	42.4	2.0	95.4	601	860	85.3	73.4

异的强度和塑性匹配,因此着重分析其拉伸断口附近的组织结构。图 6(a)为 DIA700-60 拉伸断口附近截面相图。如图所示,该区域多为块状马氏体(BCC,体积分数 92.2%),晶粒沿着轴向拉长,排列方向无显著差异,相中亚晶界大幅增多,高密度小角度晶界对应着大变形导致的强烈且均匀的位错增殖,这一点在 KAM(图 6(b))中也有体现。如图 6(c)所示,残余奥氏体为细长条状,平均晶粒尺寸为 $0.287 \mu m^2$;视场内残余奥氏体晶粒取向也呈现出一定差异,上半区晶粒取向主要为 $\langle 111 \rangle$ 和 $\langle 101 \rangle$,下半区晶粒取向相对杂乱,这也间接地反映出不同区域的奥氏体稳定性和转变程度差异。相对于未变形态(图 3(c-3)),晶粒取向未发生显著变化(图 6(d))。

图 7(a)为 DIA700-60 拉伸试样断口附近的 TEM 和选区电子衍射(SAED)照片,可以观察到明显的形变马氏体和孪晶,后者互相平行且未见交割,片层厚度约 5~15 nm。由此可见,DIA700-60 实验钢的强韧机

制主要为相变诱发塑性和孪晶诱发塑性。此外,如图 7(b)所示,黑色残余奥氏体晶粒中存在孤立的堆垛层错(从晶界贯穿整个晶粒),通常被认作位错运动的障碍,在低层错能金属和合金中对应变硬化有一定贡献^[41]。

3.2 组织演变

相对于 IA750 实验钢,虽然 DIA700-60 的 V_{RA} 相差较小(0.3%),但是其伸长率获得了大幅提升,对应着更高的 SIMT 转化率(95.4%),意味着二次低温(700 °C)临界退火优化了残余奥氏体机械稳定性分布,也必然与初始组织中元素偏析(图 2(e))存在着某种关联。如前文所述,DIA700-60 的 EBSD 相图表现出奥氏体疏密程度区域差异(见图 3(c-2)),其尺度与富锰偏析带(图 2(e))基本相当,后者难以通过轧制和高温热处理完全消除^[42]。图 8 为 DIA700-60 实验钢 Mn 和 Al 元素分布图。如图所示,富锰区中带 Mn 元素偏聚愈发明显,贫锰区内出现一定程度的 Mn 元素偏聚(图 8 中圆圈内所示),可以理解为两次临界退

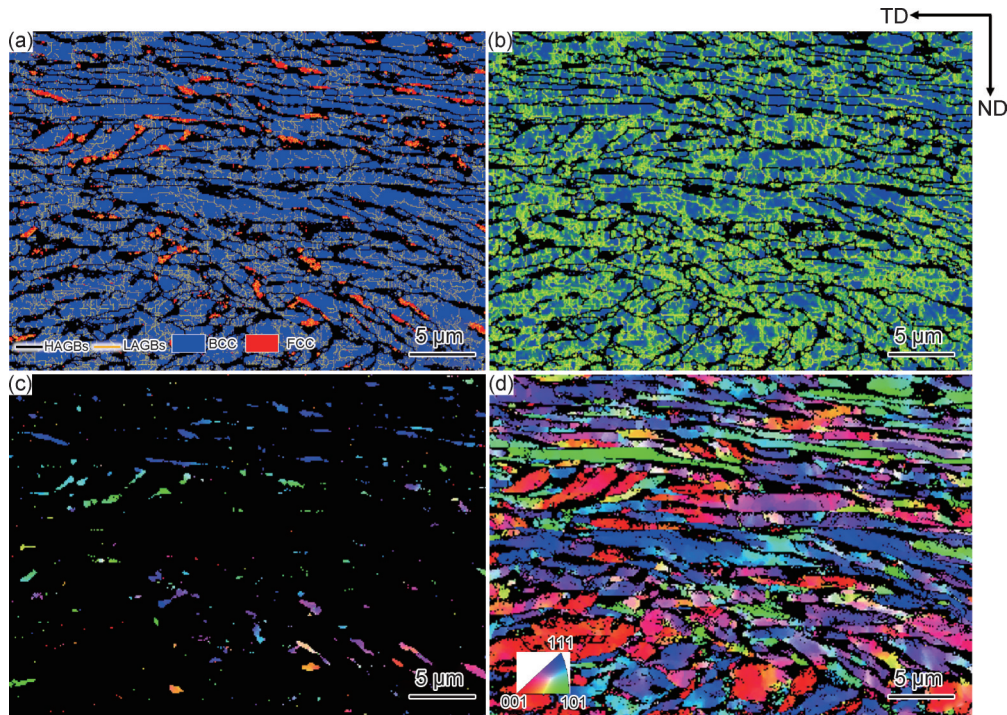


图6 DIA700-60拉伸断口的EBSD结果

(a)相图;(b)KAM图;(c)FCC相晶粒取向分布图;(d)BCC相晶粒取向分布图

Fig.6 EBSD results of DIA700-60 tensile sample adjacent to fracture

(a)phase map;(b)KAM map;(c)IPF map of FCC;(d)IPF map of BCC

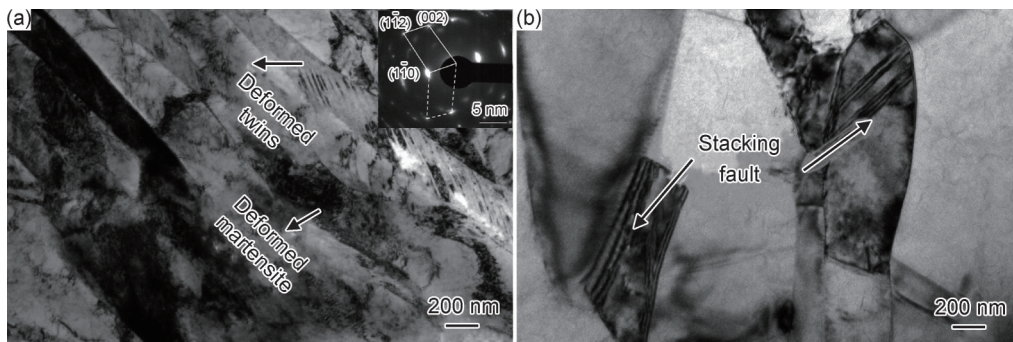


图7 DIA700-60拉伸试样断口TEM和选区电子衍射照片

(a)形变马氏体和孪晶;(b)堆垛层错

Fig.7 TEM and SAED pictures of DIA700-60 tensile sample adjacent to fracture

(a)deformed martensite and twins;(b)stacking fault

火加剧了元素配分(C/Mn由 α 或 α' 向 γ 富集)。

一般认为,热轧淬火马氏体具有较高的位错密度,在临界退火过程中经历了如下相变:(1)在升温过程中,淬火马氏体回复再结晶得到多边形铁素体^[43],碳化物在原奥氏体包界以及包内马氏体板条边界析出,而后随温度升高转变为渗碳体;(2)两相区保温初期,渗碳体不断溶解,提供奥氏体形核位点,即开始发生奥氏体逆转变;(3)随着保温时间延长,碳、锰和铝等元素跨越铁素体/奥氏体晶界或相界互相扩散,奥氏体含量增多且晶粒尺寸增大^[44]。研究表明^[45],渗碳体析出先于奥氏体逆转变,延缓了奥氏体形核;延长

保温时间,渗碳体溶解并成为奥氏体形核位点。Gu等^[46]分析了Fe-0.21C-2.0Mn-0.05Ti钢临界退火过程中组织演变,提出形核点数量的增加和马氏体基体中储存能的均匀分布,促进新的针状或块状奥氏体析出,导致晶粒细化。在较高温度(如750℃)下临界退火,渗碳体完全溶解,奥氏体逆转变程度增加,虽然提高了奥氏体含量,但晶粒长大并趋于等轴块状,奥氏体内平均C/Mn含量降低,导致奥氏体稳定性(包括化学稳定性和机械稳定性)降低、其分布范围缩小,在一定程度上不利于变形过程中获得充分和持续的TRIP效应。

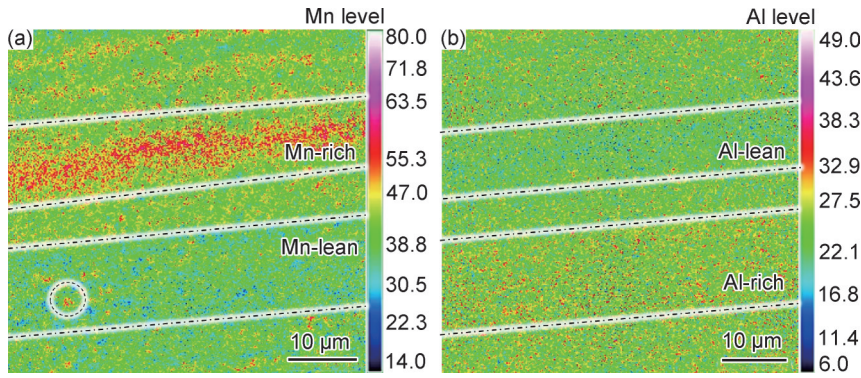


图 8 DIA700-60 实验钢的元素分布图

(a)Mn 元素分布图;(b)Al 元素分布图

Fig.8 Element distribution maps of DIA700-60 experimental steel

(a)Mn element distribution map;(b)Al element distribution map

考虑到相变行为与化学成分之间的密切关联^[47],富锰区的奥氏体逆转变程度更高,消耗淬火马氏体中的畸变储存能,抑制了铁素体回复再结晶;贫锰区发生部分奥氏体逆转变,且滞后于铁素体回复再结晶。本工作利用富锰和贫锰区淬火马氏体组织转变的细微差异,探究在不显著降低残余奥氏体含量的前提下,改善其稳定性并拓宽分布范围。图 9 为含 Mn 偏析带实验钢两步临界退火过程中的组织演变示意图,截面富锰(Mn-rich)和贫锰(Mn-lean)带显微组织分别用上半区和下半区放大图表示。热轧淬火态(HR &

quenched)初始组织包括马氏体(α'_T ,暗红条纹)和铁素体(α ,蓝色斑点)以及分布其间的极少量残余奥氏体(γ_R ,红色)晶粒(图 9(a))。

如图 9(b)所示,经过一次临界退火(IA750),富锰区板条马氏体在晶界形核,直接逆转变和快速长大,获得较为密集粗大的板条奥氏体(γ_{R-L})和临界铁素体(α_{IA}),而细粒状残余奥氏体(γ_{R-G})得以保留;贫锰区淬火马氏体先发生部分回复再结晶,再逆转变为奥氏体($\gamma_{R'}$),从而保留了板条状(γ_{R-L})或块状($\gamma_{R'-B}$)等多种形态,残余奥氏体含量相对较低。结合图 1 可知,富锰和

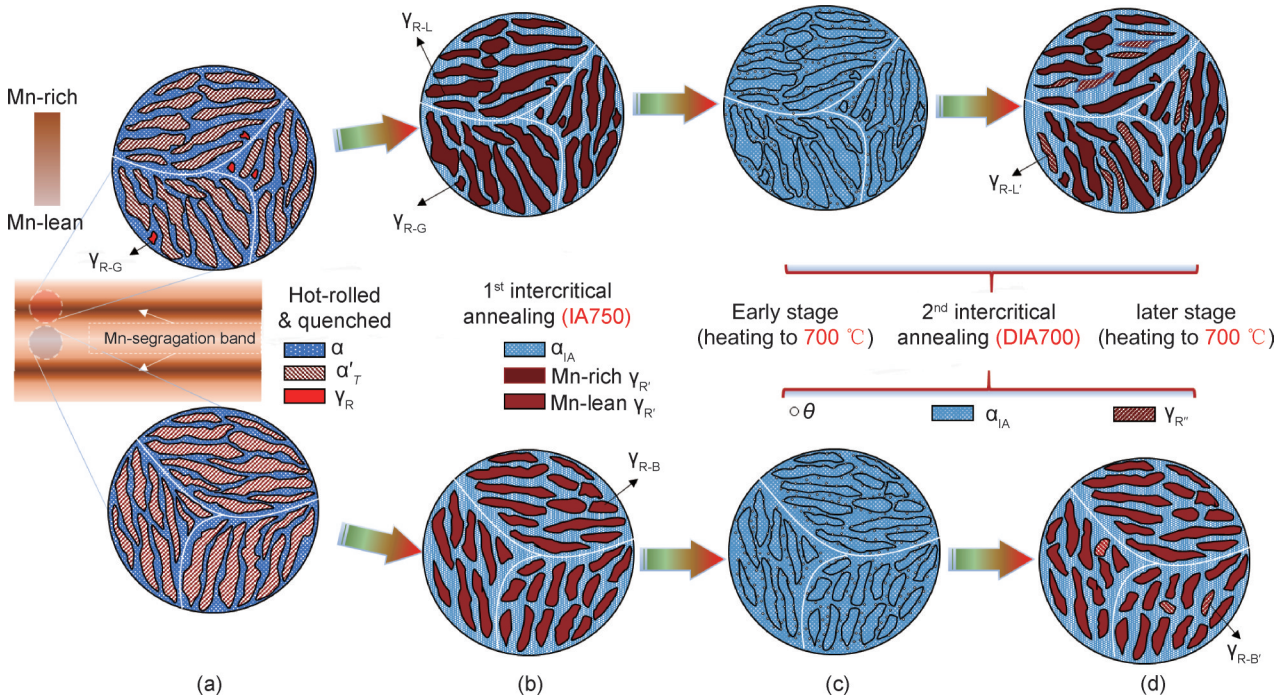


图 9 含 Mn 偏析带实验钢两步临界退火过程中组织演变示意图

(a)初始热轧态;(b)一次临界退火(750 °C保温);(c)二次临界退火前期(升温至 700 °C);(d)二次临界退火后期(700 °C保温)

Fig.9 Schematic diagrams of microstructure evolution of Mn-segregation band contained experimental steel during double intercritical annealing (a)hot-rolled and quenched state;(b)first IA at 750 °C;(c)second IA early stage(heating to 700 °C);(d)second IA later stage(holding at 700 °C)

贫锰区经一次高温(750 °C)临界退火均完成了较高度度的奥氏体逆转变,晶粒尺寸较大且分布相对均匀,保留了块状、板条、粒状等多种形态。

在两步低温(700 °C)临界退火的升温阶段,富锰区 γ_{R-L} 转变为铁素体,晶界析出大量、富C/Mn的细小渗碳体(白色点状颗粒,如图9(c)所示)。富锰区中渗碳体在后续保温过程中(见图9(c))重新溶解,作为奥氏体逆转变的形核位点,促进了无扩散生长型奥氏体逆转变,获得尺寸更细小、机械稳定性更高的板条奥氏体(γ_{R-L})和粒状残余奥氏体(γ_{R-G})^[37]。相对而言,贫锰区中析出渗碳体数量相对较少,奥氏体形核率和生长程度更低,由此产生的晶粒细化效应较小,残余奥氏体仍保留了一次临界退火时的形态和尺寸,而元素配分(C/Mn由 α 或 α' 向 γ 富集)^[48]将进一步提高其奥氏体稳定性。

如图9(d)所示,经两步临界退火处理后,贫锰区残余奥氏体含量低,且晶粒多为等轴状;而富锰区的残余奥氏体含量更高,晶粒得以细化,且保留了板条状和粒状等形态。相对于DIA700-10,当保温时间延长至60 min,渗碳体数量减少,奥氏体逆转变更加充分,适当地提高了残余奥氏体含量和机械稳定性。综上所述,富锰和贫锰区存在奥氏体含量、元素分布、晶粒尺寸和形态等异质结构特征差异,丰富并扩大了奥氏体机械稳定性分布,为基于持续、充分TRIP效应获得优异强塑性匹配创造了有利条件。

4 结论

(1)热轧淬火态中锰实验钢的初始显微组织为板条马氏体基体和极少量粒状奥氏体,存在明显的Mn偏析带;采用两步临界退火处理(750 °C×1 h + 700 °C×1 h)分阶段调控奥氏体逆转变程度,强化了富Mn区和贫Mn区的元素偏聚程度和异质结构特征,促进了残余奥氏体晶粒细化和机械稳定性的梯度分布。

(2)相对于一次高温(750 °C)临界退火,两步低温(700 °C)临界退火在不显著改变残余奥氏体含量(体积分约42%)的前提下,大幅提高了中锰实验钢的形变诱发马氏体相变转化率,通过相变/孪晶诱发塑性效应协同增韧,最终获得优异强度和韧性匹配,断后伸长率和强塑积达到85.3%和73.4 GPa·%。

参考文献

[1] MILLER R L. Ultrafine-grained microstructures and mechanical properties of alloy steels [J]. Metallurgical Transactions, 1972, 3 (4):905-912.

[2] CAI Z H, DING H, XUE X, et al. Microstructural evolution and mechanical properties of hot-rolled 11% manganese TRIP steel [J]. Materials Science and Engineering: A, 2013, 560:388-395.

[3] LEE S, LEE S J, SANTHOSH KUMAR S, et al. Localized deformation in multiphase, ultra-fine-grained 6 pct Mn transformation-induced plasticity steel [J]. Metallurgical and Materials Transactions A, 2011, 42(12):3638-3651.

[4] GIBBS P J, DE MOOR E, MERWIN M J, et al. Austenite stability effects on tensile behavior of manganese-enriched-austenite transformation-induced plasticity steel [J]. Metallurgical and Materials Transactions A, 2011, 42(12):3691-3702.

[5] LEE S, LEE S J, DE COOMAN B C. Austenite stability of ultrafine-grained transformation-induced plasticity steel with Mn partitioning [J]. Scripta Materialia, 2011, 65(3):225-228.

[6] LUO Y, PENG J M, WANG H B, et al. Effect of tempering on microstructure and mechanical properties of a non-quenched bainitic steel [J]. Materials Science and Engineering: A, 2010, 527(15):3433-3437.

[7] CAO W Q, WANG C Y, SHI J, et al. Application of quenching and partitioning to improve ductility of ultrahigh strength low alloy steel [J]. Materials Science Forum, 2010, 654/655/656:29-32.

[8] 董瀚, 王毛球, 翁宇庆. 高性能钢的M³组织调控理论与技术 [J]. 钢铁, 2010, 45(7):1-7.

DONG H, WANG M Q, WENG Y Q. Performance improvement of steels through M³ structure control [J]. Iron and Steel, 2010, 45(7):1-7.

[9] LV C, HUANG X M, WANG Y H, et al. Modulating mechanical properties of Fe-0.35C-3.2Al-5Mn hot-rolled steel by combining twinning-induced plasticity plus transformation-induced plasticity effect [J]. Steel Research International, 2022, 93(5):2100534.

[10] VAN DIJK N H, BUTT A M, ZHAO L, et al. Thermal stability of retained austenite in TRIP steels studied by synchrotron X-ray diffraction during cooling [J]. Acta Materialia, 2005, 53(20):5439-5447.

[11] JIA Q X, CHEN L, XING Z B, et al. Tailoring hetero-grained austenite via a cyclic thermomechanical process for achieving ultra-high strength-ductility in medium-Mn steel [J]. Scripta Materialia, 2022, 217:114767.

[12] SEO E J, CHO L, ESTRIN Y, et al. Microstructure-mechanical properties relationships for quenching and partitioning (Q&P) processed steel [J]. Acta Materialia, 2016, 113:124-139.

[13] XIONG X C, CHEN B, HUANG M X, et al. The effect of morphology on the stability of retained austenite in a quenched and partitioned steel [J]. Scripta Materialia, 2013, 68(5):321-324.

[14] 朱延山, 罗咪, 曲锦波. Mn含量对含铝中锰钢相变温度和显微组织的影响 [J]. 材料工程, 2023, 51(6):131-138.

ZHU Y S, LUO M, QU J B. Effect of Mn content on phase transition temperature and microstructure of Al-contained medium manganese steels [J]. Journal of Materials Engineering, 2023, 51(6):131-138.

[15] 王文芳, 潘红波, 赵淮北, 等. 合金元素对热轧中锰钢组织及力学性能的影响 [J]. 材料热处理学报, 2021, 42(4):81-86.

WANG W F, PAN H B, ZHAO H B, et al. Effect of alloying ele-

- ments on microstructure and mechanical properties of hot rolled medium manganese steel [J]. *Transactions of Materials and Heat Treatment*, 2021, 42(4): 81-86.
- [16] HU B, LUO H W. A strong and ductile 7Mn steel manufactured by warm rolling and exhibiting both transformation and twinning induced plasticity [J]. *Journal of Alloys and Compounds*, 2017, 725: 684-693.
- [17] XU Y B, HU Z P, ZOU Y, et al. Effect of two-step intercritical annealing on microstructure and mechanical properties of hot-rolled medium manganese TRIP steel containing δ -ferrite [J]. *Materials Science and Engineering: A*, 2017, 688: 40-55.
- [18] HAN J, LEE S J, JUNG J G, et al. The effects of the initial martensite microstructure on the microstructure and tensile properties of intercritically annealed Fe-9Mn-0.05C steel [J]. *Acta Materialia*, 2014, 78: 369-377.
- [19] ZHANG X L, YAN J H, LIU T, et al. Microstructural evolution and mechanical behavior of a novel heterogeneous medium Mn cold-rolled steel [J]. *Materials Science and Engineering: A*, 2021, 800: 140344.
- [20] ZOU Y, XU Y B, HU Z P, et al. Austenite stability and its effect on the toughness of a high strength ultra-low carbon medium manganese steel plate [J]. *Materials Science and Engineering: A*, 2016, 675: 153-163.
- [21] HU B, LUO H W. A novel two-step intercritical annealing process to improve mechanical properties of medium Mn steel [J]. *Acta Materialia*, 2019, 176: 250-263.
- [22] KUZMINA M, PONGE D, RAABE D. Grain boundary segregation engineering and austenite reversion turn embrittlement into toughness: example of a 9 wt.% medium Mn steel [J]. *Acta Materialia*, 2015, 86: 182-192.
- [23] CHEN H, XU X J, XU W, et al. Predicting the austenite fraction after intercritical annealing in lean steels as a function of the initial microstructure [J]. *Metallurgical and Materials Transactions A*, 2014, 45(4): 1675-1679.
- [24] NAKADA N, MIZUTANI K, TSUCHIYAMA T, et al. Difference in transformation behavior between ferrite and austenite formations in medium manganese steel [J]. *Acta Materialia*, 2014, 65: 251-258.
- [25] HAN J, LEE Y K. The effects of the heating rate on the reverse transformation mechanism and the phase stability of reverted austenite in medium Mn steels [J]. *Acta Materialia*, 2014, 67: 354-361.
- [26] LEE H, JO M C, SOHN S S, et al. Novel medium-Mn (austenite + martensite) duplex hot-rolled steel achieving 1.6 GPa strength with 20% ductility by Mn-segregation-induced TRIP mechanism [J]. *Acta Materialia*, 2018, 147: 247-260.
- [27] 陈学双, 黄兴民, 刘俊杰, 等. 一种含富锰偏析带的热轧临界退火中锰钢的组织调控及强化机制 [J]. *金属学报*, 2023, 59(11): 1448-1456.
- CHEN X S, HUANG X M, LIU J J, et al. Microstructure regulation and strengthening mechanisms of a hot-rolled & intercritical annealed medium-Mn steel containing Mn-segregation band [J]. *Acta Metallurgica Sinica*, 2023, 59(11): 1448-1456.
- [28] TSUCHIYAMA T, INOUE T, TOBATA J, et al. Microstructure and mechanical properties of a medium manganese steel treated with interrupted quenching and intercritical annealing [J]. *Scripta Materialia*, 2016, 122: 36-39.
- [29] ARLAZAROV A, GOUNE M, BOUAZIZ O, et al. Time-evolution of microstructure and mechanical behaviour of double annealed medium Mn steel [J]. *Materials Science and Technology*, 2019, 35(17): 2076-2083.
- [30] JIA Q X, CHEN L, CHEN X, et al. Enhancing strength-ductility synergy in medium Mn steel with hetero-structured austenite developed by two-stage cyclic thermomechanical treatment and flash annealing [J]. *Scripta Materialia*, 2023, 226: 115196.
- [31] IDRISSE H, RENARD K, SCHRYVERS D, et al. On the relationship between the twin internal structure and the work-hardening rate of TWIP steels [J]. *Scripta Materialia*, 2010, 63(10): 961-964.
- [32] CAI Z H, DING H, MISRA R D K, et al. Austenite stability and deformation behavior in a cold-rolled transformation-induced plasticity steel with medium manganese content [J]. *Acta Materialia*, 2015, 84: 229-236.
- [33] 朱延安, 张继明, 曲锦波, 等. 临界退火工艺对 0.3C-5Mn-3Al 超细晶钢显微组织的影响 [J]. *材料热处理学报*, 2019, 40(7): 101-108.
- ZHU Y S, ZHANG J M, QU J B, et al. Influence of intercritical annealing process on microstructure of 0.3C-5Mn-3Al ultra-fine grain steel [J]. *Transactions of Materials and Heat Treatment*, 2019, 40(7): 101-108.
- [34] KWIATKOWSKI DA SILVA A, LEYSON G, KUZMINA M, et al. Confined chemical and structural states at dislocations in Fe-9wt% Mn steels: a correlative TEM-atom probe study combined with multiscale modelling [J]. *Acta Materialia*, 2017, 124: 305-315.
- [35] 田亚强, 黎旺, 郑小平, 等. 两相区退火热轧中锰钢碳化物析出行为与组织性能研究 [J]. *材料导报*, 2019, 33(16): 2765-2770.
- TIAN Y Q, LI W, ZHENG X P, et al. Study on carbide precipitation behavior and microstructure and mechanical property of intercritically annealed hot-rolled medium manganese steel [J]. *Materials Reports*, 2019, 33(16): 2765-2770.
- [36] MORITO S, TANAKA H, KONISHI R, et al. The morphology and crystallography of lath martensite in Fe-C alloys [J]. *Acta Materialia*, 2003, 51(6): 1789-1799.
- [37] LEE S J, KIM J, KANE S N, et al. On the origin of dynamic strain aging in twinning-induced plasticity steels [J]. *Acta Materialia*, 2011, 59(17): 6809-6819.
- [38] CAI Z H, DING H, XUE X, et al. Significance of control of austenite stability and three-stage work-hardening behavior of an ultrahigh strength-high ductility combination transformation-induced plasticity steel [J]. *Scripta Materialia*, 2013, 68(11): 865-868.
- [39] CAI Z H, LI H Y, JING S Y, et al. Influence of annealing temperature on microstructure and tensile property of cold-rolled Fe-0.2C-11Mn-6Al steel [J]. *Materials Characterization*, 2018, 137: 256-262.
- [40] LI Z C, DING H, CAI Z H. Mechanical properties and austenite

- stability in hot-rolled 0.2C-1.6/3.2Al-6Mn-Fe TRIP steel [J]. *Materials Science and Engineering: A*, 2015, 639: 559-566.
- [41] DE COOMAN B C, ESTRIN Y, KIM S K. Twinning-induced plasticity (TWIP) steels [J]. *Acta Materialia*, 2018, 142: 283-362.
- [42] SCHEMMANN L, ZAEFFERER S, RAABE D, et al. Alloying effects on microstructure formation of dual phase steels [J]. *Acta Materialia*, 2015, 95: 386-398.
- [43] TSUCHIYAMA T, NATORI M, NAKADA N, et al. Conditions for grain boundary bulging during tempering of lath martensite in ultra-low carbon steel [J]. *ISIJ International*, 2010, 50 (5) : 771-773.
- [44] ARLAZAROV A, GOUNÉ M, BOUAZIZ O, et al. Evolution of microstructure and mechanical properties of medium Mn steels during double annealing [J]. *Materials Science and Engineering: A*, 2012, 542: 31-39.
- [45] LAI Q Q, GOUNÉ M, PERLADE A, et al. Mechanism of austenite formation from spheroidized microstructure in an intermediate Fe-0.1C-3.5Mn steel [J]. *Metallurgical and Materials Transactions A*, 2016, 47(7): 3375-3386.
- [46] GU X L, XU Y B, WANG X, et al. Austenite formation and mechanical behavior of a novel TRIP- assisted steel with ferrite/martensite initial structure [J]. *Materials Science and Engineering: A*, 2021, 803: 140468.
- [47] SUN W W, WU Y X, YANG S C, et al. Advanced high strength steel (AHSS) development through chemical patterning of austenite [J]. *Scripta Materialia*, 2018, 146: 60-63.
- [48] ZHANG Y J, WANG J J, XIE Z Q, et al. Microstructural characteristics and tensile behavior of a hot-rolled medium-Mn steel (0.25C-8.5Mn-0.5Si-2.5Al) processed by intercritical annealing treatment [J]. *Journal of Materials Engineering and Performance*, 2020, 29(4): 2623-2634.
-
- 基金项目:**国家自然科学基金(12272325)
收稿日期:2023-11-02; **录用日期:**2023-12-19
通讯作者:黄兴民(1980—),男,副教授,博士,主要研究方向为先进高强钢研制及服役性能评价,联系地址:四川省成都市金牛区九里堤街道二环路北一段111号西南交通大学九里校区材料科学与工程学院(610031),E-mail: xmh Huang@swjtu.edu.cn

(本文责编:齐书涵)